THE JOURNAL OF PHYSICAL CHEMISTRY B

Article

pubs.acs.org/JPCB

Hydrodynamic Effects on the Relative Rotational Velocity of Associating Proteins

Maciej Długosz*,† and Jan M. Antosiewicz‡

†Centre of New Technologies and ‡Department of Biophysics, Faculty of Physics, University of Warsaw, Żwirki i Wigury 93, 02-89 Warsaw, Poland

ABSTRACT: Hydrodynamic steering effects on the barnase−barstar association were studied through the analysis of the relative rotational velocity of the proteins. We considered the two proteins approaching each other in response to their electrostatic attraction and employed a method that accounts for the long-range and many-body character of the hydrodynamic interactions, as well as the complicated shapes of the proteins. Hydrodynamic steering effects were clearly seen when attractive forces were applied to the geometric centers of the proteins (resulting in zero torques) and the attraction acted along the line that connects centers of geometry of proteins in their crystallographic complex. When we rotated barstar relative to barnase around this line by an angle in the range from −90° to 60°, the rotational velocity arising solely from hydrodynamic interactions restored the orientation of the proteins in the crystal structure. However, because, in reality, both electrostatic forces and torques act on the proteins and these forces and torques depend on the protein−protein distance and the relative orientation of the binding partners, we also investigated more realistic situations employing continuum electrostatics calculations based on atomistic protein models. Overall, we conclude that hydrodynamic interactions aid barnase and barstar in assuming a proper relative orientation upon complex formation.

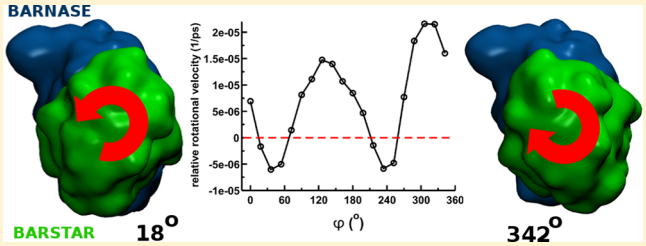

INTRODUCTION

Biochemical reactions are usually preceded by a diffusive encounter step, in which binding partners (proteins, nucleic acids, substrate molecules) approach one another through translational and rotational diffusion in a complicated force field created by the molecular environment.[1] It is well-known that two long-range interactions act between the reaction partners in the process of their encounter: electrostatic interactions and hydrodynamic interactions. Electrostatic interactions result from the fact that each molecule actually represents a certain distribution of electric charges. Strong electrostatic steering can significantly accelerate formation of the encounter complex.[2] On the other hand, hydrodynamic interactions result from the fact that each moving solute particle sets the solvent medium in motion and the resulting flux in the solvent medium then tends to move all of the other solute particles. As a consequence, hydrodynamic interactions are expected to slow the formation of encounter complexes[3−8] although under special conditions, such as molecular crowding, acceleration is predicted.[9]

Electrostatic and hydrodynamic interactions can play a pivotal role in situations where the associating molecules not only must be brought into close proximity but also must be correctly oriented in space to form an encounter complex. The role of electrostatic torques in the acceleration of certain biochemical reactions has been demonstrated.[10,11] However, the role of hydrodynamic steering effects in the case of biomolecules is less understood. Although Brune and Kim[12] suggested that hydrodynamic interactions could induce steering torques that might also play a role in achieving proper mutual orientations of molecules upon their encounter, such hydrodynamic steering effects have largely been neglected, especially in studies of molecular association that go beyond very simplified models of binding partners.

Computational methods for predicting the effects of hydrodynamic interactions between approaching molecules of an arbitrary shape on their association rate constants are far from being well established. However, methods and tools are available[13−15] that, in particular, allow one to evaluate translational and rotational velocities of quasirigid molecules approaching each other under action of electrostatic attraction with hydrodynamic interactions between the molecules taken into account. Here, we apply such an approach[14,15] to the problem of protein−protein association. We take as a model system one of the best studied protein−protein complexes, namely, that of barnase and barstar (Figure 1). Barnase is an extracellular ribonuclease, and barstar is its intracellular inhibitor. Barnase binds strongly to negatively charged RNA molecules, and its interface is very polar and contains a number of positively charged lysine and arginine residues. Barstar, on the other hand, bears a strong negative overall charge, and its interface is also negatively charged. The barnase−barstar interaction is one of the tightest known in biology, with a binding free energy of about 20 kcal mol^{-1}.[18] The barnase−barstar complex is also one of the fastest binding protein−protein complexes, with an association rate constant on the order of 10^8 M^{-1} s^{-1}.[19] In the case of barnase−barstar, the

Received: March 13, 2013
Revised: April 29, 2013
Published: April 30, 2013

dx.doi.org/10.1021/jp402534c | J. Phys. Chem. B 2013, 117, 6165−6174

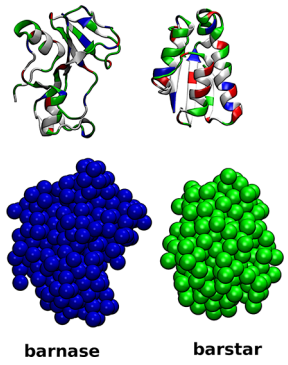

Figure 1. Barnase and barstar (PDB ID 1BGS[16]). (Top) Cartoon representations and (bottom) hydrodynamic models of the proteins (see text for details). Drawings were done with the VMD package.[17]

strong electrostatic complementarity of the interfaces enhances the binding speed over the Smoluchowski rate that applies to association by simple random search and diffusion.[20−22] Barnase−barstar binding, and, in particular, the role of electrostatic interactions, has been characterized by experiment,[18,19,23−27] continuum electrostatics calculations,[28] Brownian and Langevin dynamics simulations,[29−31] a transition state approach,[2] and molecular dynamics simulations.[32]

We focus in this work on yet another aspect of the barnase−barstar encounter, namely, the possible role of solvent-mediated hydrodynamic interactions. We employed a rigorous hydrodynamic approach that accounts for the long-range and many-body character of hydrodynamic interactions, as well as the complicated shapes of the proteins[13−15,33] and continuum electrostatics calculations performed for atomistic models of proteins to investigate hydrodynamic steering effects in the barnase−barstar system, including both their magnitude and their influence on the orientations of the approaching proteins. We believe that the picture emerging from our study, more complicated than in the case of simplified model systems that were investigated previously,[6,7,12] is quite interesting. We show that hydrodynamic interactions favor the proper relative orientation of barnase and barstar purely as a consequence of the complementary shapes of the proteins' interfaces. We observe that, depending on the mutual orientation of the binding partners, the relative rotational movement can be either slowed or accelerated (even by a factor of a few times) by hydrodynamic interactions. Moreover, the relative magnitude of hydrodynamic effects on the relative rotational velocity of the proteins depends on the ionic strength, which modulates the electrostatic forces and torques between barnase and barstar. Hydrodynamic effects can become either more or less pronounced with increasing ionic strength, depending on the instantaneous relative orientation of the binding partners.

METHODS

Hydrodynamic Interactions. Molecules that translate and rotate in a viscous fluid generate a flow field that couples their motions, and this coupling is an origin of so-called hydrodynamic interactions. For N spherical molecules suspended in an unbounded viscous fluid at low Reynolds number when creeping-flow equations are applicable, one can write the following equations relating the translational and rotational velocities of the molecules to the external forces and torques (here, by external, we also mean intermolecular interactions with other suspended molecules, such as electrostatic interactions) that act on the molecules

$$\vec{v}_i = \sum_j^N (\mu_{ij}^{\mathrm{tt}} \vec{F}_j + \mu_{ij}^{\mathrm{tr}} \vec{T}_j) \tag{1}$$

$$\vec{\omega}_i = \sum_j^N (\mu_{ij}^{\mathrm{rt}} \vec{F}_j + \mu_{ij}^{\mathrm{rr}} \vec{T}_j) \tag{2}$$

where i runs over all molecules; $\vec{v}_i$ and $\vec{\omega}_i$ are the translational and rotational velocities, respectively, of the ith molecule; and $\vec{F}_i$ and $\vec{T}_i$ are the total force and the total torque, respectively, acting on the ith molecule. Coupling of the translational (tt) and rotational (rr) motions of the molecules is introduced through mobility tensors of rank 2, denoted as μ_{ij}^{tt}, μ_{ij}^{rr}, μ_{ij}^{tr}, and μ_{ij}^{rt}. These tensors are functions of coordinates of all of the molecules in the studied system. By introducing $6N$-dimensional vectors of generalized velocities $\vec{V} = (\vec{v}_1, ..., \vec{v}_N, \vec{\omega}_1, ..., \vec{\omega}_N)$ $\vec{V}$ and forces $\vec{f} = (\vec{F}_1, ..., \vec{F}_N, \vec{T}_1, ..., \vec{T}_N)$, eqs 1 and 2 can be written compactly as

$$\vec{V} = \mathbf{M}\vec{f} \tag{3}$$

with the generalized $6N \times 6N$ mobility matrix defined as

$$\mathbf{M} = \begin{pmatrix} \mu_{11}^{\mathrm{tt}} & \cdots & \mu_{1N}^{\mathrm{tt}} & \mu_{11}^{\mathrm{tr}} & \cdots & \mu_{1N}^{\mathrm{tr}} \\ \vdots & \ddots & \vdots & \vdots & \ddots & \vdots \\ \mu_{1N}^{\mathrm{tt}} & \cdots & \mu_{NN}^{\mathrm{tt}} & \mu_{1N}^{\mathrm{tr}} & \cdots & \mu_{NN}^{\mathrm{tr}} \\ \mu_{11}^{\mathrm{rt}} & \cdots & \mu_{1N}^{\mathrm{rt}} & \mu_{11}^{\mathrm{rr}} & \cdots & \mu_{1N}^{\mathrm{rr}} \\ \vdots & \ddots & \vdots & \vdots & \ddots & \vdots \\ \mu_{N1}^{\mathrm{rt}} & \cdots & \mu_{NN}^{\mathrm{rt}} & \mu_{N1}^{\mathrm{rr}} & \cdots & \mu_{NN}^{\mathrm{rr}} \end{pmatrix} \tag{4}$$

Solutions of biological molecules can rarely be treated as solutions of spherical particles, as the shapes of proteins, nucleic acids, and other biomolecules can be highly complicated. However, an arbitrarily shaped molecule can be described from the hydrodynamic standpoint as a rigid array of spherical subunits,[33] and once the complete mobility matrix for the configuration of spheres that constitutes the hydrodynamic model of a given molecule is known, the mobility matrix for a rigid cluster consisting of these spheres can be derived.[15] This is achieved by using a projection matrix, $\mathbf{C}$, which, in the case of a single rigid conglomerate consisting of N spherical subunits, takes the form

$$\mathbf{C} = \begin{pmatrix} \mathbf{1} & (\vec{r}_c - \vec{r}_1)\times \\ \vdots & \vdots \\ \mathbf{1} & (\vec{r}_c - \vec{r}_N)\times \\ \mathbf{0} & \mathbf{1} \\ \vdots & \vdots \\ \mathbf{0} & \mathbf{1} \end{pmatrix} \tag{5}$$

where $\vec{r}_{i=1,...,N}$ is a vector of Cartesian coordinates of the ith subunit and $\vec{r}_c$ denotes the location of the center of geometry of the rigid cluster. $(\vec{r}_c - \vec{r}_i)\times$ denotes a skew-symmetric matrix

dx.doi.org/10.1021/jp402534c | J. Phys. Chem. B 2013, 117, 6165−6174

$$(\vec{r}_c - \vec{r}_i)\times = \begin{pmatrix} 0 & -(z_c - z_i) & y_c - y_i \\ z_c - z_i & 0 & -(x_c - x_i) \\ -(y_c - y_i) & x_c - x_i & 0 \end{pmatrix} \quad (6)$$

The 6 × 6 mobility matrix of a rigid cluster, $\mathbf{M}_c$, is given by

$$\mathbf{M}_c = (\mathbf{C}^T\mathbf{M}^{-1}\mathbf{C})^{-1} = \begin{pmatrix} \mu^{tt} & \mu^{tr} \\ \mu^{rt} & \mu^{rr} \end{pmatrix} \quad (7)$$

where the 3 × 3 mobility subtensors μ correspond to the translational (tt) and rotational (rr) motions of the cluster and the hydrodynamic couplings between the translations and rotations (tr/rt). In the case of a single cluster, $\mathbf{C}$ is a $6N \times 6$ matrix. For a system of N_c rigid clusters, $\mathbf{C}$ is a $N_c \times N_c$ matrix composed of submatrices given by eq 5, corresponding to different clusters, and the resulting matrix $\mathbf{M}_c$ is a $6N_c \times 6N_c$ matrix formally equivalent to the $\mathbf{M}$ matrix from eq 4, describing the mobility of N_c clusters, each composed of certain number of spherical elements. In our work, we consider a system containing two clusters, one for each of the two protein molecules, barnase and barstar. Thus, in the case studied here, $\mathbf{M}_c$ is a 12 × 12 matrix that can formally be divided into the component 3 × 3 tensors

$$\mathbf{M}_{c,12\times12} = \begin{pmatrix} \mu^{tt}_{(11)} & \mu^{tr}_{(11)} & \mu^{tt}_{(12)} & \mu^{tr}_{(12)} \\ \mu^{rt}_{(11)} & \mu^{rr}_{(11)} & \mu^{rt}_{(12)} & \mu^{rr}_{(12)} \\ \mu^{tt}_{(21)} & \mu^{tr}_{(21)} & \mu^{tt}_{(22)} & \mu^{tr}_{(22)} \\ \mu^{rt}_{(21)} & \mu^{rr}_{(21)} & \mu^{rt}_{(22)} & \mu^{rr}_{(22)} \end{pmatrix} \quad (8)$$

where subscripts 1 and 2 correspond to barnase and barstar, respectively. Subtensors $\mu_{(ii)}$ correspond to translational (tt) and rotational (rr) motions of the ith molecule and their couplings (tr/rt). Subtensors $\mu_{(ij),i\neq j}$ describe how the motions of one of the molecules (i) affect the motions of the other (j). We thus have coupling between translations of molecules (tt), rotations of molecules (rr), and their translations and rotations (tr/rt).

Translational ($\vec{v}$) and rotational ($\vec{\omega}$) velocities of the two proteins are related to the forces ($\vec{F}$) and torques ($\vec{T}$) acting on the proteins

$$\begin{pmatrix} \vec{v}_{(1)} \\ \vec{\omega}_{(1)} \\ \vec{v}_{(2)} \\ \vec{\omega}_{(2)} \end{pmatrix} = \begin{pmatrix} \mu^{tt}_{(11)} & \mu^{tr}_{(11)} & \mu^{tt}_{(12)} & \mu^{tr}_{(12)} \\ \mu^{rt}_{(11)} & \mu^{rr}_{(11)} & \mu^{rt}_{(12)} & \mu^{rr}_{(12)} \\ \mu^{tt}_{(21)} & \mu^{tr}_{(21)} & \mu^{tt}_{(22)} & \mu^{tr}_{(22)} \\ \mu^{rt}_{(21)} & \mu^{rr}_{(21)} & \mu^{rt}_{(22)} & \mu^{rr}_{(22)} \end{pmatrix} \begin{pmatrix} \vec{F}_{(1)} \\ \vec{T}_{(1)} \\ \vec{F}_{(2)} \\ \vec{T}_{(2)} \end{pmatrix} \quad (9)$$

If the hydrodynamic interactions resulting from the relative motions of the two rigid molecules were neglected, eq 9 would take the form

$$\begin{pmatrix} \vec{v}_{(1)} \\ \vec{\omega}_{(1)} \\ \vec{v}_{(2)} \\ \vec{\omega}_{(2)} \end{pmatrix} = \begin{pmatrix} \mu^{tt,o}_{(11)} & \mu^{tr,o}_{(11)} & \mathbf{0} & \mathbf{0} \\ \mu^{rt,o}_{(11)} & \mu^{rr,o}_{(11)} & \mathbf{0} & \mathbf{0} \\ \mathbf{0} & \mathbf{0} & \mu^{tt,o}_{(22)} & \mu^{tr,o}_{(22)} \\ \mathbf{0} & \mathbf{0} & \mu^{rt,o}_{(22)} & \mu^{rr,o}_{(22)} \end{pmatrix} \begin{pmatrix} \vec{F}_{(1)} \\ \vec{T}_{(1)} \\ \vec{F}_{(2)} \\ \vec{T}_{(2)} \end{pmatrix} \quad (10)$$

where superscripts o signify that the single-molecule mobility subtensors are, in general, different from the corresponding subtensors in eq 9—yet another consequence of the omission of hydrodynamic interactions between the two rigid clusters.

In our work, we employ the HYDROLIB library,[14] a numerical implementation that calculates the mobility matrix for a collection of equally sized spheres suspended in an incompressible viscous fluid. The spheres can be arranged in a number of rigid arrays,[15] and the evaluation of the mobility matrix for a suspension of such rigid clusters can also be performed with HYDROLIB. HYDROLIB utilizes the method of induced forces, an efficient scheme proposed in ref 13 that addresses the three fundamental difficulties inherent in the evaluation of hydrodynamic interactions, namely, their long-range, many-body character; their short-range divergence; and the associated lubrication effects.[13,34,35]

Hydrodynamic Models of Proteins. We constructed hydrodynamic models of barnase and barstar using an approach similar to that described in ref 15. Each protein is described as a set of touching spheres with equal radii of 2 Å (291 spheres in the case of barnase and 246 spheres in the case of barstar). The centers of the spheres are positioned on nodes of the hexagonal-closed-packed lattice and enclosed within the solvent-accessible surface of the protein (Figure 1).

Electrostatic Interactions. For the purposes of the current study, we assumed that the forces and torques acting on the proteins (eqs 9 and 10) result from intermolecular interactions and are electrostatic in origin.

We created atomistic protein models based on the X-ray structure of the barnase−barstar complex[16] (Figure 1). We used the PROPKA utility[36] with the CHARMM PARAM22 parameter set[37] to add hydrogens to the heavy atoms of the proteins with the solution pH set to 8.0.[18] Partial charges and radii were assigned with the PDB2PQR tool.[38] The resulting total protein net charges were $+2e$ for barnase and $-6e$ for barstar.

Interactions between barnase and barstar were evaluated with the effective-charge approach.[39,40] We derived effective charges positioned at the heavy atoms of the proteins by fitting the electrostatic potential resulting from the Debye−Hückel approximation[41] to the external molecular potential obtained as a numerical solution of the linearized Poisson−Boltzmann equation.[42] The electrostatic potentials of barnase and barstar were computed using APBS[43] at ionic strengths of 0.05, 0.10, and 0.15 M with the dielectric constants of the proteins and the solvent set to 2 and 78.54, respectively, with protein structures generated by PDB2PQR[38] and PROPKA.[36] Effective charges were obtained by solving numerically the system of linear equations

$$\mathbf{A}\vec{q} = \vec{b} \quad (11)$$

where $\vec{q}$ represents the vector of effective charges, the $\mathbf{A}$ matrix is defined as

dx.doi.org/10.1021/jp402534c | J. Phys. Chem. B 2013, 117, 6165−6174

$$A_{ij} = \int_{\Omega} d^3\vec{r}\ \frac{\exp(-\kappa|\vec{r} - \vec{r}_i|)}{\varepsilon|\vec{r} - \vec{r}_i|}\frac{\exp(-\kappa|\vec{r} - \vec{r}_j|)}{\varepsilon|\vec{r} - \vec{r}_j|} \quad (12)$$

and the elements of $\vec{b}$ are given by

$$b_i = \int_{\Omega} d^3\vec{r}\ \frac{\exp(-\kappa|\vec{r} - \vec{r}_i|)}{\varepsilon|\vec{r} - \vec{r}_i|}\Phi^{PB}(\vec{r}) \quad (13)$$

In these equations, Ω denotes the volume outside a molecule where the electrostatic potential is fitted, $\Phi^{PB}(\vec{r})$ is the value of the electrostatic potential at a given point $\vec{r}$ obtained by numerically solving the linearized Poisson–Boltzmann equation, ε is the dielectric constant of the solvent, and κ is the inverse of the Debye length. The volume Ω was defined as a 5-Å-thick skin around a protein with the lower boundary of the skin determined as the van der Waals surface of the protein inflated by 3 Å. The quality of the effective-charge fits was described with the accuracy parameter, χ

$$\chi = 1 - \frac{\int_{\Omega} d^3\vec{r}\ |\Phi^{PB}(\vec{r}) - \sum q_j \frac{\exp(-\kappa|\vec{r} - \vec{r}_j|)}{\varepsilon|\vec{r} - \vec{r}_j|}|^2}{\int_{\Omega} d^3\vec{r}\ |\Phi^{PB}(\vec{r})|^2} \quad (14)$$

In the cases of both barnase and barstar, we were able to fit the effective charges with χ values greater than 0.99. Using potential-derived effective charges, the electrostatic forces acting between barnase and barstar were computed as

$$\vec{F}_{ij} = \frac{q_i q_j}{\varepsilon r_{ij}^2}\exp(-\kappa r_{ij})(1 + \kappa r_{ij})\frac{\vec{r}_{ij}}{r_{ij}} \quad (15)$$

where q_i denotes the effective charges of barnase, q_j denotes the effective charges of barstar, and r_{ij} denotes their mutual distances.

Evaluation of Rotational Velocities. We generated a set of barnase–barstar configurations using the procedure schematically depicted in Figure 2. Starting from the crystallographic complex, barstar was translated away from barnase, along the line that connects the geometric centers of the proteins in their complex, by different distances ΔR. Additionally, for each value of ΔR, barstar was rotated around the same line by an angle ϕ that covers the range from 0° to 360° in regular intervals of 18°. The minimum value of ΔR was set to 11 Å so that, regardless of the value of the rotation angle ϕ, no overlap would occur between the hydrodynamic models of the proteins. Some example barnase–barstar configurations are given in Figure 3. The translation of barstar along the line connecting the centers of the proteins in the crystallographic complex that we applied to generate barnase–barstar configurations is consistent with the results of Brownian dynamics simulations conducted for this system by Spaar et al.[29] They found that the barnase–barstar binding free energy surface has a funnel-like shape and that the last stage of binding proceeds orthogonally to the interfaces of the proteins. Moreover, Wang et al.[32] characterized the one-dimensional potential of mean force for the dissociation process of the barnase–barstar complex by biased molecular dynamics simulations also using the center-to-center distance of the proteins as a reaction coordinate.

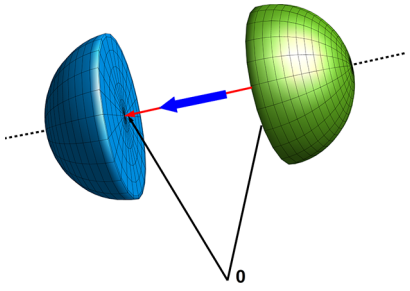

Figure 2. Transformations of protein coordinates performed to generate barnase–barstar configurations for which the rotational velocities of the proteins were evaluated. Hemispheres represent barnase (blue) and barstar (green). The vector connecting the geometric centers of the proteins in their crystallographic complex is shown in red (pointing toward barnase). We generated different configurations of proteins by translating barstar along the line that connects centers of the proteins and rotating barstar around this line. The blue arrow pointing toward barnase denotes the rotational velocity of barstar that would result from the direction of barstar's successive rotations around the line connecting the centers of the proteins.

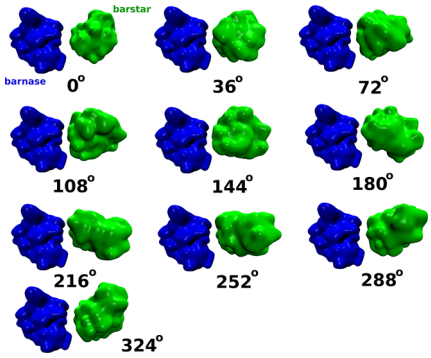

Figure 3. Example barnase–barstar configurations. In all of the configurations, barstar is translated by ΔR = 15 Å from its position in the crystallographic complex. The value of the barstar rotation angle ϕ is given for each configuration (see also Figure 2). Proteins are depicted using their molecular surfaces (constructed for hydrodynamic models of barnase and barstar with the QuickSurf VMD algorithm[17]).

For each barnase–barstar configuration described with particular values of ΔR and ϕ, we evaluated the 12 × 12 mobility matrix for the two proteins together (eq 9), as well as the 6 × 6 mobility matrices for barnase and barstar separately (eq 10). The latter were computed for each protein–protein configuration. The mobility matrix was evaluated relative to the geometric center of the cluster, and its components were affected by rotations of the cluster around its center of geometry, but not by translations. For each barnase–barstar configuration from the generated set, we thus obtained a set of three mobility matrices: a 12 × 12 matrix that describes the translational and rotational mobilities of the two rigid clusters and their hydrodynamic couplings and the two 6 × 6 mobility matrices for barnase and barstar, each describing translational and rotational mobilities of a given protein in the absence of the other protein.

For each barnase–barstar configuration from the generated set, we computed the total electrostatic forces (eq 15) and the total moments of the electrostatic forces acting on the proteins at different ionic strengths. The total torque acting on barnase (barstar) was computed relative to the geometric center of the barnase (barstar) hydrodynamic model.

Using the 12 × 12 mobility matrices, the electrostatic forces and torques, and eq 9, we evaluated the velocities of barnase and barstar for each configuration in the generated set. The

dx.doi.org/10.1021/jp402534c | J. Phys. Chem. B 2013, 117, 6165–6174

obtained velocities result from barnase−barstar electrostatic interactions and take into account the hydrodynamic interactions between the two proteins. Next, we evaluated the rotational velocities of the proteins in the absence of hydrodynamic interactions for each barnase−barstar configuration in the generated set using eq 10 and the computed 6 × 6 mobility matrices. The velocities were evaluated with the solvent viscosity set to 1 cP.

To analyze the hydrodynamic effects in the studied system, we employed the projection of the rotational velocity of barstar (measured in the barnase-fixed frame) onto the unitary vector parallel to the vector that connects the centers of geometry of the proteins in their crystallographic complex (Figure 2), $\Omega_{\parallel}$.

RESULTS

Hydrodynamic Steering Effects in the Dumbbell−Dumbbell System. Although the focus of our work is the hydrodynamic effects on the association of proteins of complicated shapes, we also investigated a much simpler case, namely, that of two similar hydrodynamic dumbbells, each composed of equally sized (with 5-Å radii) touching spheres. We describe this system for the sake of illustration of the hydrodynamic effects and as a reference to previous studies[6,7,12] that employed equally simplified model molecules.

We generated a set of dumbbell−dumbbell configurations following the procedure depicted in Figure 2. Initially, the dumbbells were oriented in a parallel fashion (i.e., the skew angle measured between the long axes of the dumbbells was set to 0°) with the line connecting their centers perpendicular to the long axes of both dumbbells. The distance between the centers of the dumbbells was fixed at 20 Å. We assumed that equal forces with directions resulting in dumbbell−dumbbell attraction act on the centers of the dumbbells along the line connecting the centers of the dumbbells. Moreover, the torques acting on the dumbbells were set to zero. When there are no hydrodynamic interactions between them, the dumbbellsdo not rotate relative to each other (see eq 10)—first, because there is no coupling between the motions of the two dumbbells and, second, because of the dumbbell's symmetry. However, when hydrodynamic interactions are taken into account with eq 9, a relative rotational motion of the dumbbells arises. The rotational motion occurs in the plane perpendicular to the line of their centers. Figure 4 presents the projection of the rotational velocity of one of the dumbbells (green hemisphere in Figure 2) measured in the frame fixed on the second dumbbell (blue hemisphere in Figure 2) onto the unit vector parallel to the vector connecting the centers of the dumbbells (red arrow in Figure 2), $\Omega_{\parallel}$. From the data given in Figure 4, one can conclude that the rotations arising from the hydrodynamic coupling between the dumbbells always occur in a direction that leads to the restoration of the perpendicular orientation of dumbbells. Pushing the dumbbell−dumbbell pair together results in their being more favorable oriented for the perpendicular encounter, an effect that arises solely because of the hydrodynamic interactions between the dumbbells. Similar observations were described previously in refs 6, 7, and 12. Although the model system described here is somewhat primitive, the hydrodynamic effect that is shown might be of biological relevance, especially when one considers the binding of molecules having complementary shapes, as suggested in ref 12. Whenever the binding partners are pushed together, they become more favorably oriented for the reaction by the hydrodynamic interactions between their complementary shapes.

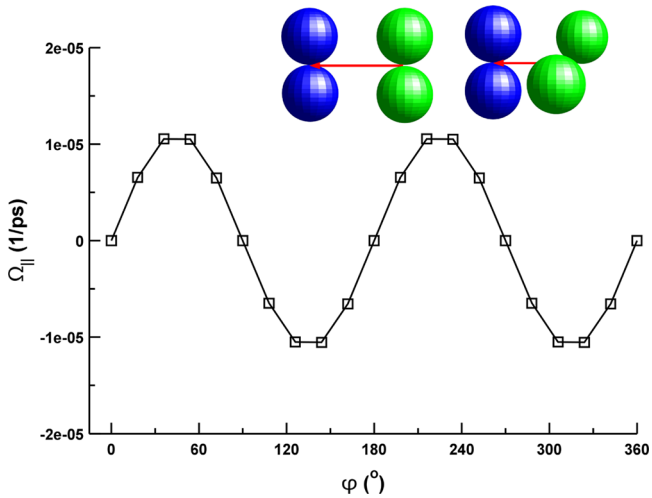

Figure 4. Projection of the relative rotational velocity of the dumbbells onto the unit vector parallel to the vector connecting the centers of the dumbbells (see also Figure 2), $\Omega_{\parallel}$, obtained for different rotation angles, ϕ. In all depicted cases, attractive forces of similar magnitudes (1 kcal mol^{-1} Å^{-2}), acting along the line connecting the centers of the dumbbells, are assumed. The torques acting on the dumbbells are set to zero. Calculations were performed using eq 9.

Hydrodynamic Steering Effects in the Barnase−Barstar System. After analyzing the dumbbell−dumbbell system, we investigated the role of hydrodynamic orientational effects in the barnase−barstar system in a similar fashion. We modeled both proteins as rigid clusters of equal touching spheres, obtaining reasonable approximations of their shapes (see Figures 1 and 3).

Focusing on effects related to the shapes of the proteins, we evaluated the rotational velocities of the proteins that would arise assuming their relative configurations described with particular values of ΔR and ϕ, if the proteins were to be pushed together along the line connecting their centers of geometry by constant intermolecular forces, assuming that the total torques acting on the proteins due to these forces are zero. Without hydrodynamic interactions, when the motions of the proteins are uncoupled (see eq 10), the rotational velocities of both proteins are negligible. However, the hydrodynamic coupling introduced with eq 9 results in substantial relative rotations of the proteins. Figure 5 depicts $\Omega_{\parallel}$ as a function of the rotation angle ϕ for different barnase−barstar distances. The curves depicted in Figure 5 have similar character, with minima observed for values of the rotation angle of 45° and 240° and maxima observed for ϕ values of around 130° and 315°. The dependence of the absolute value of $\Omega_{\parallel}$ on ΔR is clearly visible, and with increasing barnase−barstar distance, the absolute $\Omega_{\parallel}$ value becomes smaller. As for all values of ΔR given in Figure 5, the attractive forces acting on proteins are of the same magnitude, the differences observed in $\Omega_{\parallel}$ with increasing ΔR result from the properties of hydrodynamic interactions,[13,34,35] namely, their short-range and long-range behaviors. [To give the reader a better idea of how close the two proteins approach each other in the generated set of their relative configurations, in Table 1, we present minimum surface-to-surface distances obtained for hydrodynamic models of the proteins for ΔR = 11 Å and different values of ϕ.) The sign of $\Omega_{\parallel}$ corresponds to the direction of barstar's rotations (around the line of centers,

dx.doi.org/10.1021/jp402534c | J. Phys. Chem. B 2013, 117, 6165−6174

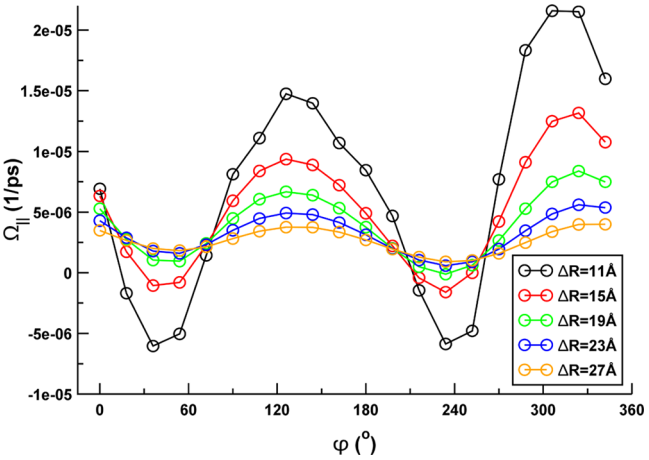

Figure 5. Projection of the relative rotational velocity of the proteins onto the unit vector parallel to the vector connecting the centers of the proteins in the crystallographic complex (see also Figure 2), $\Omega_{||}$, obtained for different barnase–barstar configurations (ΔR, ϕ). In all depicted cases, attractive forces of similar magnitudes (1 kcal mol^{-1} Å^{-2}), acting on the geometric centers of the proteins along the line connecting the geometric centers of the proteins, are assumed, whereas the torques acting on the proteins are set to zero. Calculations were performed using eq 9.

Table 1. Minimum Surface-to-Surface Distances of Barnase and Barstar in Relative Configurations with ΔR = 11 Å and Different Values of Barstar's Rotation Angle, ϕ

ϕ (deg)	distance (Å)	ϕ (deg)	distance (Å)
0	3.99	180	2.17
18	3.13	198	2.70
36	3.11	216	2.81
54	3.27	234	2.24
72	2.81	252	1.31
90	2.62	270	0.76
108	2.19	288	1.82
126	1.93	306	3.60
144	2.20	324	3.40
162	1.61	342	3.43

relative to barnase) that arises because of the hydrodynamic interactions between barnase and barstar as they are pushed together by attractive forces. Negative values correspond to rotations in the direction opposite to the direction of the rotations performed to generate the barnase–barstar configurations (see Figure 2). Although the dependence of $\Omega_{||}$ on ϕ is more complicated than that observed in the simple dumbbell–dumbbell scenario, the hydrodynamic complementarity of the shapes of the proteins is clearly visible. For values of the barstar rotation angle ϕ up to about 60°, the rotations induced by the hydrodynamic interactions help to restore the crystallographic configuration of the proteins, as the values of $\Omega_{||}$ are negative. However, this is true only for values of ΔR less than 19 Å. Above this ΔR value, we observed that the induced rotations act to further distort the relative orientation of the proteins. For values of ϕ above 270°, we again observed that the hydrodynamic interactions act so as to bring the two proteins closer to their crystal configurations with positive values of $\Omega_{||}$; this was observed for all values of ΔR investigated. Whereas, in the case of the dumbbell–dumbbell system that we described in the previous section, the rotations arising from hydrodynamic interactions always (for all values of ϕ) restore the perpendicular orientation of dumbbells, in the case of the barnase–barstar complex, the aiding effect of hydrodynamic interactions is observed for only a limited range of ϕ values, as the interfaces of the proteins are complicated and the complementarity of their shapes is local rather than global.

In the preceding scenario, constant and attractive forces are applied to the centers of the proteins resulting in zero torques. However, in reality, intermolecular forces resulting from electrostatic interactions between binding partners depend on their relative configuration as well as conditions such as the solution ionic strength, and they result in nonzero electrostatic torques acting on each of the two proteins. We thus investigated the barnase–barstar system employing continuum electrostatics calculations to evaluate their interactions. In Tables 2 and 3, we present details regarding the barnase–barstar electrostatic interactions in the generated configurations. Regardless the value of the barstar rotation angle ϕ and the solution ionic strength, the total force acting at the barstar center is attractive (barstar is pushed toward barnase), as all projections of the total force ($F_{||}$) given in Table 2 are positive. Moreover, if one considers the magnitudes of the total force given in Table 2, the total forces acting on the centers of the proteins are almost collinear with the vector that connects the geometric centers of the proteins (Figure 2). The barnase–barstar electrostatic interactions result in nonzero torques as detailed in Table 3.

Table 2. Projection of the Vector of the Total Electrostatic Force Acting at Barstar's Center onto the Unit Vector Parallel to the Vector Connecting the Centers of the Proteins in Their Crystallographic Complex,[a] $F_{||}$ (kcal mol^{-1} Å^{-2}), along with the Magnitudes of the Total Force, F (kcal mol^{-1} Å^{-2}, in Parentheses)[b,c]

	I (M)		
ϕ (deg)	0.05	0.10	0.15
0	0.24 (0.26)	0.23 (0.24)	0.21 (22)
18	0.23 (0.25)	0.21 (0.23)	0.19 (22)
36	0.24 (0.27)	0.23 (0.25)	0.21 (24)
54	0.23 (0.26)	0.21 (0.24)	0.20 (23)
72	0.19 (0.23)	0.18 (0.21)	0.16 (19)
90	0.15 (0.19)	0.13 (0.17)	0.12 (0.16)
108	0.12 (0.16)	0.11 (0.14)	0.09 (0.12)
126	0.17 (0.19)	0.15 (0.17)	0.14 (0.15)
144	0.22 (0.25)	0.21 (0.23)	0.20 (0.22)
162	0.24 (0.29)	0.23 (0.27)	0.22 (0.25)
180	0.24 (0.30)	0.23 (0.28)	0.21 (0.26)
198	0.22 (0.28)	0.21 (0.26)	0.19 (0.25)
216	0.21 (0.26)	0.19 (0.24)	0.17 (0.22)
234	0.22 (0.25)	0.20 (0.23)	0.18 (0.22)
252	0.25 (0.27)	0.23 (0.25)	0.21 (0.23)
270	0.29 (0.30)	0.27 (0.28)	0.25 (0.26)
288	0.30 (0.30)	0.28 (0.29)	0.27 (0.27)
306	0.31 (0.32)	0.30 (0.30)	0.28 (0.28)
324	0.30 (0.31)	0.29 (0.29)	0.27 (0.28)
342	0.28 (0.29)	0.26 (0.27)	0.25 (0.25)

[a]See Figure 2. [b]Calculations were performed for ΔR = 11 Å. [c]For comparison, the magnitude of the Coulombic force between two elementary point charges placed within a distance of 1 Å in a dielectric medium with ε = 78.54 is 4.22 kcal mol^{-1} Å^{-2}.

We calculated the electrostatic forces and torques acting on the two proteins in each of their relative configurations in the

dx.doi.org/10.1021/jp402534c | J. Phys. Chem. B 2013, 117, 6165–6174

Table 3. Normalized Electrostatic Torques Acting on Barnase and Barstar at Different Ionic Strengths for Different Values of Barstar's Rotation Angle, ϕ, at ΔR = 11 Å

		barnase			barstar		
I (M)	ϕ (deg)	T_x/T	T_y/T	T_z/T	T_x/T	T_y/T	T_z/T
0.05	0	0.933	0.355	−0.048	−0.154	−0.942	0.298
	90	0.927	0.351	−0.127	0.312	−0.946	0.081
	180	0.901	0.338	−0.269	−0.936	0.244	0.251
	270	0.915	0.345	−0.207	−0.873	−0.393	0.288
0.1	0	0.933	0.355	−0.05	−0.211	−0.938	0.272
	90	0.928	0.352	−0.117	−0.008	−0.993	0.116
	180	0.903	0.339	−0.263	−0.936	0.244	0.251
	270	0.913	0.343	−0.221	−0.893	−0.369	0.256
0.15	0	0.933	0.355	−0.053	−0.238	−0.936	0.258
	90	0.929	0.352	−0.113	−0.231	−0.964	0.133
	180	0.905	0.339	−0.257	−0.937	0.235	0.257
	270	0.911	0.343	−0.227	−0.902	−0.357	0.241

generated set and at different ionic strengths, and then we evaluated the rotational velocities of barnase and barstar in their different relative configurations, either taking hydrodynamic interactions into account (eq 9) or neglecting them altogether (eq 10). Some of the resulting values of $\Omega_{\|}$ are given in Figure 6. As one might expect, given the dependence of electrostatic

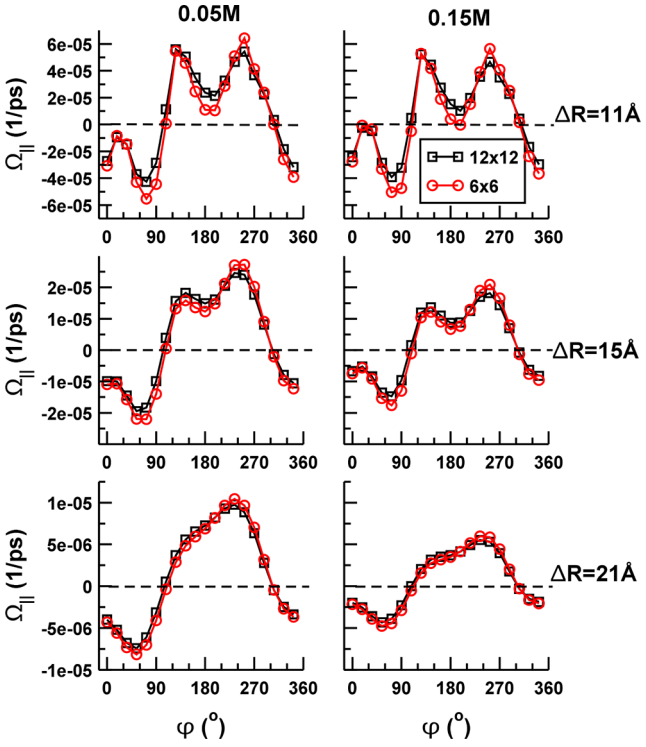

Figure 6. Values of $\Omega_{\|}$ obtained for different barnase−barstar configurations at different ionic strengths. Calculations either took the hydrodynamic interactions between barnase and barstar into account (eq 9, squares) or neglected these interactions completely (eq 10, circles).

interactions on the mutual distance between proteins, the value of $\Omega_{\|}$ was found to decrease with increasing distance ΔR, regardless of the treatment of the hydrodynamic interactions. The shape of the $\Omega_{\|}$ curves also changes with increasing ΔR. Most notably, the minimum observed at ϕ = 180° vanishes for ΔR = 21 Å. Switching on the hydrodynamic interactions does not change the direction of barstar's rotations (in the barnase-fixed frame) in comparison with the situation when hydrodynamic interactions are neglected. However, one can clearly see that, depending on the ϕ value, the hydrodynamic interactions either decrease ($\phi \approx 90°$, $\phi \approx 270°$) or increase ($\phi \approx 180°$) the rate of barstar's rotations. Moreover, the magnitude of the steering effects of these hydrodynamic interactions appears to be dependent on ΔR and the ionic strength. To evaluate the relative magnitude of the hydrodynamic effects on the rotational velocities of barnase and barstar, we computed values of the ratio $1 - (\Omega_{\|}^{12\times12})/(\Omega_{\|}^{6\times6})$ (where the superscript 12 × 12 correspond to the situation when hydrodynamic interactions are taken into account and the superscript 6 × 6 corresponds to the situation when hydrodynamic interactions are neglected) for different relative barnase−barstar configurations at different ionic strengths. Figure 7 depicts $1 - (\Omega_{\|}^{12\times12})/(\Omega_{\|}^{6\times6})$ as a function of ΔR for ϕ

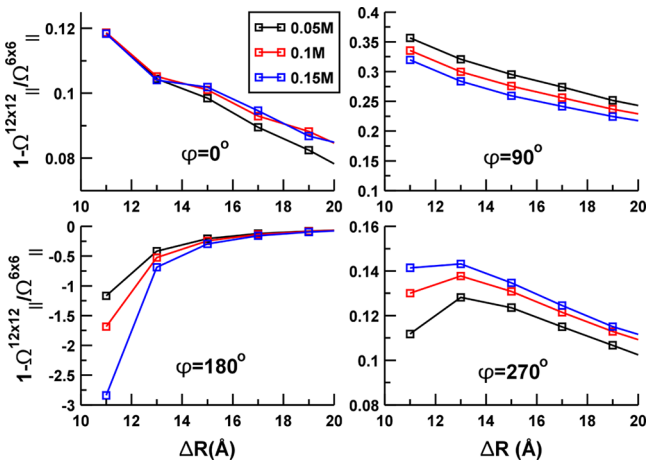

Figure 7. Relative magnitude of hydrodynamic effects on $\Omega_{\|}$ for different ionic strengths and different barnase−barstar configurations (ΔR, ϕ).

= 0° (barnase and barstar oriented as in the crystallographic complex), 90°, 180°, and 270° and three values of the ionic strength. In all cases, the magnitude of the hydrodynamic effects decreases with increasing ΔR. Only a small influence in hydrodynamic interactions is observed for ϕ = 0°, with relative rotational velocities being decreased by about 10%. However, the effects of the hydrodynamic interactions become slightly

dx.doi.org/10.1021/jp402534c | J. Phys. Chem. B 2013, 117, 6165−6174

more pronounced with increasing ionic strength. A similar magnitude and behavior of the hydrodynamic effects were observed in the case of ϕ = 270°. For ϕ = 90°, the hydrodynamic effects are more visible (about 30% decrease in the relative rotational velocity). However, in this case, the magnitude of the hydrodynamic effects decreases with increasing ionic strength. The magnitude of the hydrodynamic effects is much larger in the case of ϕ = 180°. Notably, switching on the hydrodynamics interactions in this case results in an increase of the relative rotational velocity of the proteins, even by 300% at short protein−protein distances. For ϕ = 180°, the magnitude of the hydrodynamic effects decreases with decreasing ionic strength.

DISCUSSION

Since the pioneering works of Kramers,[44] Debye,[45] and Friedman,[3] it has been known that the rates of diffusional encounters of molecules participating in chemical reactions are influenced by electrostatic and hydrodynamic interactions. In principle, the mechanism by which these interactions influence the diffusional encounters of reaction partners is well understood: Direct electrostatic intermolecular forces and moments of these forces add deterministic translational and rotational velocities to the underlying random translational and rotational motions, and subsequently, the translational and rotational velocities induced by deterministic and random forces are modified by hydrodynamic interactions. Initially, the quantitative evaluation of the effects of electrostatic and hydrodynamic interactions was limited to simple models of reacting molecules. Substantial progress in the evaluation of the effects of electrostatic interactions on the reactions of molecules of arbitrary shapes and electric charge distributions was made possible by the introduction of numerical methods for the solution of the Poisson−Boltzmann equation for solute−solvent systems.[46] On the other hand, quantitative evaluation of the effects of hydrodynamic interactions on the rates of diffusional encounters is still available only for simple models of reacting molecules.[3−8,47] However, it is possible to predict the effects of hydrodynamic interactions on the translational and rotational velocities of arbitrary-shaped molecules modeled by aggregates of an arbitrary number of spherical elements, using rigorous hydrodynamic approaches.[13,14] In this work, we employed such an approach, as well as continuum electrostatics calculations, to investigate hydrodynamic steering effects on protein−protein association. We used the well-studied[2,18,19,23−32] barnase−barstar complex as a model system. We accounted for the complicated shapes of the proteins as well as the long-range and many-body character of the hydrodynamic interactions.[13−15] Although we consider a two-body system, many-body hydrodynamic interactions between N frictional elements that constitute the models of the proteins are properly taken into account in the $6N \times 6N$ mobility matrix (eq 4) and in the resulting two-body 12×12 mobility matrix (eq 8).[13] At this point, we should acknowledge that, whereas the hydrodynamic approach applied in this work provides a high level of accuracy in the case of suspensions of spheres and their clusters,[13,15] the modeling of complicated shapes of biological molecules as assemblies of spherical frictional elements (beads) has its limitations. Because we use hydrodynamic models consisting of touching beads of equal sizes, we are not able to describe proteins at atomic resolution. For that purpose, we would need models that consist of overlapping beads of unequal sizes, and no accurate treatment of such bead models exists. An alternative to the approach used in this work is the boundary element method.[48] Based on an exact integral form of the Stokes equations for the velocity field outside an aribtrarily shaped body,[49] this method focuses on the surface of the modeled molecule, thereby avoiding the problems inherent in bead models. Modern implementations of the boundary element method allow for a solution of the Stokes equations in the case of very detailed models of biomolecular surfaces, leading to impressively accurate predictions of the diffusion tensors of molecules.[50,51] To our knowledge, so far, only single molecules have been modeled with such state-of-the-art implementations of the boundary element method.[50−52]

Because the effects of hydrodynamic interactions investigated in the present work arise in response to movements of the particles caused by direct electrostatic forces and their moments, it is difficult to separate orientational effects arising solely from hydrodynamic interactions from those due to electrostatic torques. Therefore, as our first step, we considered a situation in which an artificial attractive force acts on the centers of the proteins while setting the torques acting on the proteins to zero. We concluded that the complementarity of the shapes of barnase and barstar can result in their being more favorably oriented for reaction by hydrodynamic interactions. The effects of such a complementarity are local rather than global, and we observed that hydrodynamic interactions act to properly orient the approaching proteins when the value of their relative rotation angle, ϕ, is above 270° regardless of their mutual distance (Figure 5). Additionally, when the distance between the approaching proteins becomes sufficiently small, the orienting effect of hydrodynamic interactions is visible also for ϕ values below 60° (Figure 5). However, when we considered the two proteins oriented as in the crystal structure (ϕ = 0°), we found that a nonzero relative rotational velocity arises as a result of their hydrodynamic interactions (Figure 5). In the case of the simple model system consisting of two hydrodynamic dumbbells (Figure 4), we observed that the relative rotational velocity (and thus the hydrodynamic steering effect) vanishes when the two dumbbells are oriented in a perpendicular fashion, an orientation that is optimal from the hydrodynamic standpoint. For the much more complicated shapes of barnase and barstar, the relative orientation that would result in vanishing relative rotational velocity seems to be shifted by a few degrees from that observed in their crystal structure. However, one should keep in mind that, in all barnase−barstar configurations that we evaluated, the two proteins were farther apart than in their crystal structure to avoid steric hindrance. We are aware that we probably cannot describe the behavior of proteins at close contact when excluded-volume interactions and local rearrangements of side chains come into play. Additionally, as we described previously, bead models are not able to achieve atomistic description of proteins and our hydrodynamic models of barnase and barstar certainly miss some finer-level details of the interfaces of the proteins and subtle effects of hydration or molecular conformation.

When we considered more realistic electrostatic interactions between the two proteins (forces and torques resulting from their charge distributions), we observed that the hydrodynamic effects depend strongly on the relative configurations of the approaching proteins. The relative rotations of the two binding partners induced by electrostatic torques can be further either slowed or accelerated by hydrodynamic effects (Figure 7), and these effects depend on both the electrostatic forces and the

dx.doi.org/10.1021/jp402534c | J. Phys. Chem. B 2013, 117, 6165−6174

electrostatic torques that act on the proteins in their particular configuration. The relative magnitude of hydrodynamic effects on the relative rotational velocity of the two proteins also depends on the solution ionic strength (Figure 7). Interestingly, we observed that, when the approaching proteins are oriented so that the value of the relative rotation angle ϕ falls in the range from 150° to 210°, the relative rotational velocity of the proteins is increased by hydrodynamic interactions even by a factor of 4 (Figures 6 and 7), whereas for values of ϕ outside this range, only a moderate decrease in rotational velocities is visible. It thus appears that hydrodynamic interactions help barnase and barstar to achieve a proper orientation upon binding by either slowing their relative rotation (and thus allowing the proteins to establish favorable intermolecular contacts) when their configuration is close to the native one or by accelerating their relative rotation when their orientation is far from the native one. The latter effect is rather short-ranged (Figure 7) and vanishes quickly with increasing distance between the proteins.

We note that we have neglected the fact that solvated proteins undergo random Brownian movement arising from collisions with solvent molecules, which would be required in a full Brownian dynamics simulation of the diffusional encounter process. Such calculations are not feasible at present, as the memory- and time-consuming procedure of computation of the mobility matrices by the equations presented in the Methods section would need to be done at each time step of such simulations. However, the inclusion of Brownian motions would not change the conclusions of this work.

AUTHOR INFORMATION

Corresponding Author

*E-mail: mdlugosz@cent.uw.edu.pl. Phone: +48 22 5540 821. Fax: +48 22 5540 801.

Notes

The authors declare no competing financial interest.

ACKNOWLEDGMENTS

The authors acknowledge support from National Science Centre (N N519 646640).

REFERENCES

(1) Schreiber, G.; Haran, G.; Zhou, H. X. Fundamental Aspects of Protein−Protein Association Kinetics. *Chem. Rev.* **2009**, *109*, 939−860.

(2) Alsallq, R.; Zhou, H. X. Electrostatic Rate Enhancement and Transient Complex of Protein−Protein Association. *Proteins* **2008**, *71*, 320−335.

(3) Friedman, H. L. A Hydrodynamic Effect in the Rates of Diffusion Controlled Reactions. *J. Phys. Chem.* **1966**, *70*, 3931−3933.

(4) Deutch, J. M.; Felderhof, B. U. Hydrodynamic Effect in Diffusion-Controlled Reaction. *J. Chem. Phys.* **1973**, *59*, 1669−1671.

(5) Wolynes, P. G.; Deutch, J. M. Slip Boundary Conditions and the Hydrodynamic Effect on Diffusion Controlled Reactions. *J. Chem. Phys.* **1976**, *65*, 450−454.

(6) Antosiewicz, J.; Briggs, J. M.; McCammon, J. A. Orientational Steering in Enzyme−Substrate Association: Ionic Strength Dependence of Hydrodynamic Torque Effects. *Eur. Biophys. J.* **1996**, *24*, 137−141.

(7) Antosiewicz, J.; McCammon, J. A. Electrostatic and Hydrodynamic Orientational Steering Effects in Enzyme−Substrate Association. *Biophys. J.* **1995**, *69*, 57−65.

(8) Shushin, A. I. Influence of Hydrodynamic Interaction on the Diffusion-Controlled Reaction Kinetics of Molecules with Highly Anisotropic Reactivity. *J. Chem. Phys.* **2003**, *118*, 1301−1311.

(9) Wojciechowski, M.; Szymczak, P.; Cieplak, M. The Influence of Hydrodynamic Interactions on Protein Dynamics in Confined and Crowded Spaces—Assessment in Simple Models. *Biol. Phys.* **2010**, *7*, 046011.

(10) Luty, B. A.; Wade, R. C.; Madura, J. D.; Davis, M. E.; Briggs, J. M.; McCammon, J. A. Brownian Dynamics Simulations of Diffusional Encounters between Triose Phosphate Isomerase and Glyceraldehyde Phosphate: Electrostatic Steering of Glyceraldehyde Phosphate. *J. Phys. Chem.* **1993**, *97*, 233−237.

(11) Wade, R. C.; Luty, B. A.; Demchuk, E.; Madura, J. D.; Davis, M. E.; Briggs, J. M.; McCammon, J. A. Simulation of Enzyme−Substrate Encounter with Gated Active Sites. *Nat. Struct. Biol.* **1994**, *1*, 65−69.

(12) Brune, D.; Kim, S. Hydrodynamic Steering Effects in Protein Association. *Proc. Natl. Acad. Sci. U.S.A.* **1994**, *91*, 2930−2934.

(13) Cichocki, B.; Felderhof, B. U.; Hinsen, K.; Wajnryb, E.; Bławździewicz, J. Friction and Mobility of Many Spheres in Stokes Flow. *J. Chem. Phys.* **1994**, *100*, 3780−3790.

(14) Hinsen, K. HYDROLIB: A Library for the Evaluation of Hydrodynamic Interactions in Colloidal Suspensions. *Comput. Phys. Commun.* **1995**, *88*, 327−340.

(15) Cichocki, B.; Hinsen, K. Stokes Drag on Conglomerates of Spheres. *Phys. Fluids* **1995**, *7*, 285−291.

(16) Guillet, V.; Lapthorn, A.; Hartley, R. W.; Mauguen, Y. Recognition between a Bacterial Ribonuclease, Barnase, and Its Natural Inhibitor, Barstar. *Structure* **1993**, *1*, 165−176.

(17) Humphrey, W.; Dalke, A.; Schulten, K. VMD—Visual Molecular Dynamics. *J. Mol. Graphics* **1996**, *14*, 33−38.

(18) Schreiber, G. A.; Ferscht, A. R. Interaction of Barnase with Its Polypeptide Inhibitor Barstar Studied by Protein Engineering. *Biochemistry* **1993**, *32*, 5145−5150.

(19) Schreiber, G.; Fersht, A. R. Energetics of Protein−Protein Interactions: Analysis of the Barnase−Barstar Interface by Single Mutations and Double Mutant Cycles. *J. Mol. Biol.* **1995**, *248*, 478−486.

(20) Dong, F.; Vijayakumar, M.; Zhou, H. X. Comparison of Calculation and Experiment Implicates Significant Electrostatic Contributions to the Binding Stability of Barnase and Barstar. *Biophys. J.* **2003**, *85*, 49−60.

(21) Vijayakumar, M.; Wong, K. Y.; Schreiber, G.; Fersht, A. R.; Szabo, A.; Zhou, H. X. Electrostatic Enhancement of Diffusion-Controlled Protein−Protein Association: Comparison of Theory and Experiment on Barnase and Barstar. *J. Mol. Biol.* **1998**, *278*, 1015−1024.

(22) Lee, L. P.; Tidor, B. Optimization of Binding Electrostatics: Charge Complementarity in the Barnase−Barstar Protein Complex. *Protein Sci.* **2001**, *10*, 362−377.

(23) Sekatskii, S. K.; Favre, M.; Dietler, G.; Mikhailov, A. G.; Klinov, D. V.; Lukash, S. V.; Deyev, S. M. Force Spectroscopy of Barnase−Barstar Single Molecule Interaction. *J. Mol. Recognit.* **2010**, *23*, 583−588.

(24) Mitkevicha, V. A.; Schulgab, A. A.; Ermolyukb, Y. S.; Lobachov, V. M.; Chekhov, V. O.; Yakovlev, G. I.; Hartley, R. W.; Pace, C. N.; Kirpichnikov, M. P.; Makarov, A. A. Thermodynamics of Denaturation of Complexes of Barnase and Binase with Barstar. *Biophys. Chem.* **2003**, *105*, 383−390.

(25) Makarov, A. A.; Protasevich, I. I.; Lobachov, V. M.; Kirpichnikov, M. P.; Yakovlev, G. I.; Gillib, R. M.; Briandb, C. M.; Hartley, R. W. Thermostability of the Barnase−Barstar Complex. *FEBS Lett.* **1994**, *354*, 251−254.

(26) Zhuravleva, A.; Korzhnev, D. M.; Nolde, S. B.; Kay, L. E.; Arseniev, A. S.; Billeter, M.; Orekhov, V. Y. Propagation of Dynamic Changes in Barnase upon Binding of Barstar: An NMR and Computational Study. *J. Mol. Biol.* **2007**, *367*, 1079−1092.

(27) Frisch, C.; Fersht, A. R.; Schreiber, G. Experimental Assignment of the Structure of the Transition State for the Association of Barnase and Barstar. *J. Mol. Biol.* **2001**, *308*, 69−77.

(28) Wang, T.; Tomic, S.; Gabdoulline, R. R.; Wade, R. C. How Optimal Are the Binding Energetics of Barnase and Barstar? *Biophys. J.* **2004**, *87*, 1618−1630.
(29) Spaar, A.; Dammer, C.; Gabdoulline, R. R.; Wade, R. C.; Helms, V. Diffusional Encounter of Barnase and Barstar. *Biophys. J.* **2006**, *90*, 1913−1924.
(30) Gabdoulline, R. R.; Wade, R. C. Simulation of the Diffusional Association of Barnase and Barstar. *Biophys. J.* **1997**, *72*, 1917−1929.
(31) Schluttig, J.; Almanova, D.; Helms, V.; Schwartz, U. S. Dynamics of Protein−Protein Encounter: A Langevin Equation Approach with Reaction Patches. *J. Chem. Phys.* **2008**, *129*, 155106.
(32) Wang, L.; Siu, S. W. I.; Gu, W.; Helms, V. Downhill Binding Energy Surface of the Barnase−Barstar Complex. *Biopolymers* **2010**, *93*, 977−985.
(33) Garcia de la Torre, J.; Huertas, M. L.; Carrasco, B. Calculation of Hydrodynamic Properties of Globular Proteins from Their Atomic Level Structure. *Biophys. J.* **2000**, *78*, 719−730.
(34) Jeffrey, D. J.; Onishi, Y. Calculation of the Resistance and Mobility Functions for Two Unequal Rigid Spheres in Low-Reynolds-Number Flow. *J. Fluid Mech.* **1984**, *139*, 261−290.
(35) Bossis, G.; Brady, J. F. Dynamic Simulation of Sheared Suspensions. I. General Method. *J. Chem. Phys.* **1984**, *80*, 5141−5155.
(36) Li, H.; Robertson, A. D.; Jensen, J. H. Very Fast Empirical Prediction and Interpretation of Protein pK_a Values. *Proteins* **2005**, *61*, 704−721.
(37) MacKerell, A. D., Jr.; Bashford, D.; Dunbrack, R. L., Jr.; Evanseck, J. D.; Field, M. J.; Fischer, S.; Gao, J.; Guo, H.; Ha, S.; Joseph-McCarthy, D.; Kuchnir, L.; Kuczera, K.; Lau, F. T. K.; Mattos, C.; Michnick, S.; Ngo, T.; Nguyen, D. T.; Prodhom, B.; Reiher, W. E., III; Roux, B.; Schlenkrich, M.; Smith, J. C.; Stote, R.; Straub, J.; Watanabe, M.; Wiórkiewicz-Kuczera, J.; Yin, D.; Karplus, M. All-Atom Empirical Potential for Molecular Modeling and Dynamics Studies of Proteins. *J. Phys. Chem. B* **1998**, *102*, 3586−3616.
(38) Dolinsky, T. J.; Czodrowski, P.; Li, H.; Nielsen, J. E.; Jensen, J. H.; Klebe, G.; Baker, N. A. PDB2PQR: Expanding and Upgrading Automated Preparation of Biomolecular Structures for Molecular Simulations. *Nucleic Acids Res.* **2007**, *35*, W522−W525.
(39) Gabdoulline, R. R.; Wade, R. C. Effective Charges for Molecules in Solvent. *J. Phys. Chem.* **1996**, *100*, 3868−3878.
(40) Beard, D. A.; Schlick, T. Modeling Salt-Mediated Electrostatics of Macromolecules: The Discrete Surface Charge Optimization Algorithm and Its Application to the Nucleosome. *Biopolymers* **2001**, *58*, 106−115.
(41) Bell, G. M.; Levine, S.; McCartney, L. N. Approximate Methods of Determining the Double-Layer Free Energy of Interaction between Two Charged Colloidal Spheres. *J. Colloid Interface Sci.* **1970**, *33*, 335−359.
(42) Gilson, M. K.; Honig, B. Energetics of Charge−Charge Interactions in Proteins. *Proteins: Struct., Funct., Genet.* **1988**, *3*, 32−52.
(43) Baker, N. A.; Sept, J. D.; Joseph, S.; Holst, M. J.; McCammon, J. A. Electrostatics of Nanosystems: Application to Microtubules and the Ribosome. *Proc. Natl. Acad. Sci. U.S.A.* **2001**, *98*, 10037−10041.
(44) Kramers, H. A. Brownian Motion in a Field of Force and the Diffusion Model of Chemical Reactions. *Physica* **1940**, *7*, 284−304.
(45) Debye, P. Reaction Rates in Ionic Solutions. *Trans. Electrochem. Soc.* **1942**, *82*, 265−272.
(46) Warwicker, J.; Watson, H. C. Calculation of the Electric Potential in the Active Site Cleft due to α-Helix Dipoles. *J. Mol. Biol.* **1982**, *157*, 671−679.
(47) Frembgen-Kesner, T.; Elcock, A. H. Absolute Protein−Protein Association Rate Constants from Flexible, Coarse-Grained Brownian Dynamics Simulations: The Role of Intermolecular Hydrodynamic Interactions in Barnase−Barstar Association. *Biophys. J.* **2010**, *99*, L75−L77.
(48) Youngren, G. K.; Acrivos, A. Stokes Flow Past a Particle of Arbitrary Shape: A Numerical Method of Solution. *J. Fluid Mech.* **1975**, *69*, 377−402.
(49) Wegener, W. A. On an Exact Starting Expression for Macromolecular Hydrodynamic Models. *Biopolymers* **1986**, *25*, 627−637.
(50) Aragon, S. R. A Precise Boundary Element Method for Macromolecular Transport Properties. *J. Comput. Chem.* **2004**, *25*, 1191−1205.
(51) Aragon, S. R. Recent Advances in Macromolecular Hydrodynamic Modeling. *Methods* **2011**, *54*, 101−114.
(52) Allison, S. A. Low Reynolds Number Transport Properties of Axisymmetric Particles Employing Stick and Slip Boundary Conditions. *Macromolecules* **1999**, *32*, 5304−5312.